HHS Public Access

Author manuscript

Mol Cell. Author manuscript; available in PMC 2016 October 01.

Published in final edited form as:

Mol Cell. 2015 October 1; 60(1): 47–62. doi:10.1016/j.molcel.2015.08.009.

SPG7 is an Essential and Conserved Component of the Mitochondrial Permeability Transition Pore

Santhanam Shanmughapriya[1,2,5], **Sudarsan Rajan**[1,2,5], **Nicholas E. Hoffman**[1,2], **Andrew M. Higgins**[1,2], **Dhanendra Tomar**[1,2], **Neeharika Nemani**[1,2], **Kevin J. Hines**[1,2], **Dylan J. Smith**[1,2], **Akito Eguchi**[1,2], **Sandhya Vallem**[1,2], **Farah Shaikh**[1,2], **Maggie Cheung**[1,2], **Nicole J. Leonard**[1,2], **Ryan S. Stolakis**[1,2], **Matthew P. Wolfers**[1,2], **Jessica Ibetti**[2,3], **J. Kurt Chuprun**[2,3], **Neelakshi R. Jog**[1,2], **Steven R. Houser**[4], **Walter J. Koch**[2,3], **John W. Elrod**[2,3], and **Muniswamy Madesh**[1,2,4,*]

[1]Department of Biochemistry, Temple University School of Medicine, Philadelphia, Pennsylvania 19140, USA

[2]Center for Translational Medicine, Temple University School of Medicine, Philadelphia, Pennsylvania, 19140, USA

[3]Department of Pharmacology, Temple University School of Medicine, Philadelphia, Pennsylvania 19140, USA

[4]Cardiovascular Research Center, Temple University School of Medicine, Philadelphia, Pennsylvania 19140, USA

SUMMARY

Mitochondrial permeability transition is a phenomenon in which the mitochondrial permeability transition pore (PTP) abruptly opens resulting in mitochondrial membrane potential ($\Delta\Psi_m$) dissipation, loss of ATP production, and cell death. Several genetic candidates have been proposed to form the PTP complex however the core component is unknown. We identified a necessary and conserved role for spastic paraplegia 7 (SPG7) in Ca^{2+} and ROS-induced PTP opening using RNAi based screening. Loss of SPG7 resulted in higher mitochondrial Ca^{2+}, similar to cyclophilin D (CypD, *PPIF*) knockdown with sustained $\Delta\Psi_m$ during both Ca^{2+} and ROS stress. Biochemical analyses revealed that the PTP is a hetero-oligomeric complex composed of VDAC, SPG7 and

*To whom correspondence should be addressed: Muniswamy Madesh, Department of Biochemistry, 950 MERB, 3500 N. Broad Street, Temple University, Philadelphia, PA 19140, Phone: (215) 707 5465, Fax: (215) 707 9890, madeshm@temple.edu.

[5]These authors contributed equally to this manuscript.

AUTHOR CONTRIBUTIONS

S.S., S.R., N.E.H., D.T., K.J.H., D.J.S., S.V. and M.M. performed and analyzed experiments involving RNAi Screening, biochemical, molecular and cellular experiments. S.R., A.M.H., R.S.S., and M.P.W. performed molecular cloning and Y2H experiments. S.S., S.R., and N.N. performed FPLC experiments. S.S., N.E.H., D.T., A.E., F.S., M.C., and N.J.L. performed confocal imaging experiments and analysis. Flow-cytometry experiments were performed by S.S. and N.R.J. NRVM cell isolation and culture guidance were provided by J.I., J.K.C., S.R.H. and W.J.K. S.S., S.R., N.E.H and M.M. conceived, designed, and interpreted experimental data. S.S., S.R., N.E.H and M.M. wrote the manuscript with contributions from J.W.E.

The authors declare that they have no competing interests.

CypD. Silencing or disruption of SPG7-CypD binding prevented Ca^{2+} and ROS-induced $\Delta\Psi_m$ depolarization and cell death. This study identifies a ubiquitously expressed IMM integral protein, SPG7, as a core component of the PTP at the OMM and IMM contact site.

Graphical Abstract

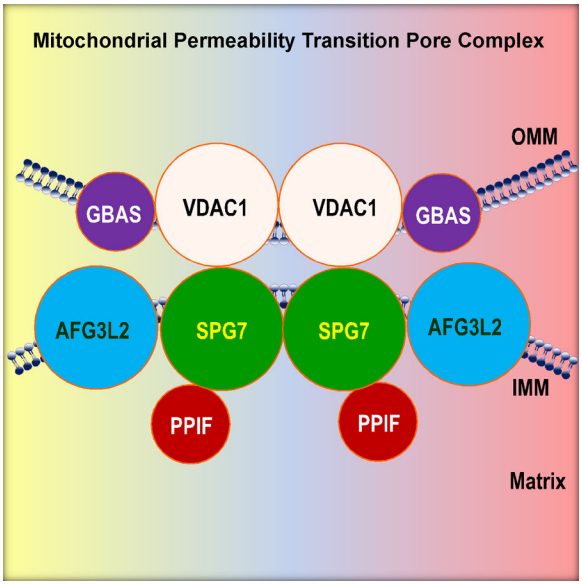

INTRODUCTION

Mitochondrial function plays a critical role in providing not only the majority of the cell's ATP but also as the pathophysiological phenotypic source of major cell death mechanisms (Newmeyer and Ferguson-Miller, 2003). Mitochondrial Ca^{2+} ($[Ca^{2+}]_m$) overload promotes the opening of the mitochondrial permeability transition pore (PTP) leading to bioenergetic crisis and cell death (Bernardi, 1999; Duchen, 2000; Halestrap et al., 1993). Though the identity of the pore is unknown, known inducers of the PTP include Ca^{2+} and reactive oxygen species (ROS). PTP opening is characterized by a decoupling of electrochemical potential ($\Delta\Psi_m$) across the inner mitochondrial membrane (IMM) which results in mitochondrial matrix osmotic disequilibrium, perturbation of Ca^{2+} handling, and ATP depletion (Bernardi, 1999; Kroemer et al., 2007). PTP opening has been implicated in several necrosis model systems and pathological states such as ischemia/reperfusion injury, cerebral stroke, and myocardial infarction (Kroemer et al., 2007). Since then, multiple proteins have been proposed to play a role in PTP opening by Ca^{2+} or ROS challenge, but of these, only CypD is regarded as a bona fide component while others remain controversial. For example, studies have suggested the outer mitochondrial membrane (OMM) proteins, voltage-dependent anion channel (VDAC), peripheral benzodiazepine receptor, hexokinase, the IMM proteins, adenine nucleotide translocase (ANT), mitochondrial phosphate carrier, and the soluble matrix peptidyl prolyl isomerase F, cyclophilin D (*PPIF*) (Elrod et al., 2010; Kroemer et al., 2007). Recently, the F_1F_o ATP synthase was shown to be involved in PTP opening (Alavian et al., 2014; Bonora et al., 2013; Giorgio et al., 2013). Additionally, a tumor suppressor, p53, was shown to translocate to the mitochondria upon oxidative stress,

interact with CypD, and elicit PTP opening (Vaseva et al., 2012). However, genetic silencing approaches have only confirmed PPIF as essential for Ca^{2+}-sensitive PTP opening (Baines et al., 2005; Nakagawa et al., 2005; Schinzel et al., 2005).

To identify the molecular components of the PTP complex in an unbiased manner, an experimental system using HEK293T and HeLa cells was developed in which expression of mitochondrial proteins were individually silenced by shRNA and evaluated for Ca^{2+} and ROS-induced PTP opening. Here, we report the identification of SPG7 as a key component of Ca^{2+} and ROS-induced PTP opening in multiple cell types. We further demonstrate that the SPG7 KD was able to handle a large number of Ca^{2+} pulses, similar to PPIF KD, with or without oxidant treatment. Our complementary protein-protein interaction studies revealed that SPG7 (IMM) recruits CypD (matrix) and VDAC1 (OMM). Importantly, we show that SPG7/CypD-dependent PTP opening and the binding of CypD and SPG7 were cyclosporine A (CsA) sensitive. SPG7 thus represents a conserved core component that constitutes the PTP complex and regulates its function.

RESULTS

Silencing 14 of 128 Mitochondrial Proteins Significantly Enhanced Mitochondrial Ca^{2+} Retention in Human Cells

To search for PTP components, we designed a shRNA based loss-of-function screen for Ca^{2+} and ROS desensitization by measuring $[Ca^{2+}]_m$ retention and $\Delta\Psi_m$. A total of 128 candidates were selected to include transmembrane, previously proposed PTP components, and less-studied mitochondrial proteins (Table S1) (Pagliarini et al., 2008; Smith et al., 2012). Stable knockdown was achieved in HEK293T cells by evaluating three to five different lentiviral shRNAs for each candidate gene. The levels of target mRNA reduction in the clones selected for further experiments were between 80–90% compared with negative shRNA (Neg shRNA) (Table S1). To examine the role of individual target genes in PTP opening, a series of 10 μM Ca^{2+} boluses was delivered to cells in which the plasma membrane was permeabilized by digitonin allowing direct access to mitochondria in the presence of thapsigargin to exclude ER Ca^{2+} uptake (Hoffman et al., 2013). A spectrofluorometer was used to detect the changes in $[Ca^{2+}]_m$ retention and $\Delta\Psi_m$ during repeated Ca^{2+} pulses (Ichas et al., 1997; Mallilankaraman et al., 2012b). Upon exposure to excessive Ca^{2+}, Neg shRNA expressing 293T cells exhibited rapid $\Delta\Psi_m$ collapse due to Ca^{2+}-induced PTP opening (Figure 1A and B). This assay confirmed that excessive matrix Ca^{2+} promotes mitochondrial depolarization and dissipation of electrochemical potential (Nakagawa et al., 2005; Williams et al., 2013). Puromycin-selected, stably expressing shRNA cells were subjected to a similar protocol to measure $[Ca^{2+}]_m$ retention and $\Delta\Psi_m$ simultaneously (Mallilankaraman et al., 2012b). For loss of PTP function, PPIF knockdown cells were used as a positive control and showed increased $[Ca^{2+}]_m$ retention compared to Neg shRNA (~22 pulses versus ~9 pulses) (Figure 1A and 1D). Of the experimental group, 14 clones (ANT2, PPIF, AFG3L2, SLC25A30, PMPCA, CHCHD3, GBAS, C10orf10, C18orf19, C6orf203, SPG7, CCDC58, MAVS and VDAC1) exhibited robust $[Ca^{2+}]_m$ retention capacity with sustained $\Delta\Psi_m$ maintenance suggesting a link between these candidates and Ca^{2+}-dependent PTP opening (Figure 1C–1P and Figure S1).

SPG7, CypD, and VDAC1 Emerge as Putative PTP Components

Besides excessive $[Ca^{2+}]_m$ overload, mitochondrial PTP opening is modulated by oxidants (Crompton, 1999; Halestrap, 2009). Therefore, we asked whether 14 PTP candidates that handled more Ca^{2+}, were also resistant to oxidant sensitization in combination with excessive $[Ca^{2+}]_m$ while maintaining $\Delta\Psi_m$. To explore the hypothesized inducible interplay of PTP opening by Ca^{2+} and ROS, 293T cells were challenged with hydrogen peroxide (H_2O_2) then assayed for sensitization to Ca^{2+}-induced PTP opening. These permeabilized cells were pretreated with H_2O_2 (8 mM) for 250 s prior to external Ca^{2+} pulses. We compared the PTP phenotype of 14 KD candidates without and with oxidant pretreatment and analyzed $[Ca^{2+}]_m$ retention and $\Delta\Psi_m$ during Ca^{2+} pulses similar to Figure 1. Neg shRNA cells exposed to oxidant pretreatment exhibited rapid Ca^{2+}-potentiated $\Delta\Psi_m$ depolarization (blue trace) when compared to experiments lacking H_2O_2 (black trace) (Figure 2A, 2P and 2Q). Remarkably, cells lacking SPG7, PPIF, and VDAC1 were indifferent to the oxidant pretreatment, handling a similar number of Ca^{2+} pulses without or with oxidant pretreatment (Figure 2C, 2L, 2O, 2P and 2Q). Although GBAS KD cells exhibited similar $[Ca^{2+}]_m$ retention with or without oxidant pretreatment, the $[Ca^{2+}]_m$ retention (13 pulses) was lower than PPIF KD cells (20 pulses). Importantly, stable knockdowns did not affect mitochondrial morphology with the exception of SPG7 (elongated) (Figure S2A and 2B). We next asked if the elongated phenotype of SPG7 KD contributed to increased $[Ca^{2+}]_m$ retention. To test this, we measured $[Ca^{2+}]_m$ retention in wild-type cells overexpressing mitochondrial fission dominant negative $Drp1^{K38A}$, known to result in elongated mitochondria (Cereghetti et al., 2008; Frank et al., 2001; Smirnova et al., 2001). As expected $Drp1^{K38A}$ overexpression resulted in elongated mitochondria (Figure S2C–2E). However, $[Ca^{2+}]_m$ retention was unchanged between wild-type, wild-type + Drp1, and wild-type + $Drp1^{K38A}$ (Figure S2F) in contrast to SPG7 KD cells suggesting that SPG7's elongated mitochondrial morphology is not a determinant of PTP opening. Collectively, these results indicate that loss of SPG7, PPIF, and VDAC1 alleviated ROS-sensitized, Ca^{2+}-induced PTP opening.

SPG7 Interacts with PTP Matrix Regulatory Component CypD and OMM Resident VDAC1

Based on results from Ca^{2+} and ROS-induced PTP opening, we sought to identify proteins associated with CypD in the mitochondria. We first generated C-terminal tagged CypD-HA and Flag-tagged 13 genes of interest. Individual candidate genes were transiently transfected in COS-7 cells, and cell lysates were subjected to immunoprecipitation with HA-antibody. Transfection of COS-7 cells with these tagged proteins showed considerable ectopic protein expression (Figure S3A, left). The Flag-tagged as well as HA-tagged individual protein cell lysates were incubated with antibodies specific for HA to immunoprecipitate the protein complexes. HA-tagged CypD protein was immunoprecipitated, while Flag-tagged candidate proteins did not pull-down demonstrating antibody specificity (Figure S3A, right). Next, we cotransfected PPIF-HA with Flag-tagged 13 candidate proteins in COS-7 cells. Only a 89 kDa molecular weight SPG7-Flag protein band was observed by immunoprecipitation using a HA-antibody in cells cotransfected with PPIF-HA + SPG7-Flag (Figure S3B, top right) (Atorino et al., 2003; Casari et al., 1998). Notably, no interaction was seen between CypD and ANT2 nor CypD and VDAC1 (Figure S3B, top right).

To further confirm the interaction between CypD and the putative PTP component SPG7, SPG7-HA was cotransfected with the remaining Flag-tagged 13 candidate proteins in COS-7 cells. As expected, ~20 kDa CypD pulled-down using an antibody specific for HA in cells cotransfected with SPG7-HA (Figure S3C, top right). In addition, HA antibody immunoprecipitated a known SPG7 binding partner AFG3L2 (Atorino et al., 2003) (Figure S3C, top right). VDAC1 was also associated with SPG7 indicating that IMM transmembrane protein SPG7 is in close proximity to the OMM (Figure S3C, top right). These results show that SPG7 interacts with CypD in the matrix and with VDAC1 possibly at IMM and OMM contact sites.

To further explore VDAC1 and SPG7 interaction, we coexpressed VDAC1-HA with Flag-tagged plasmid constructs in COS-7 cells and immunoprecipitated VDAC1 with anti-HA antibodies. The Flag-tagged SPG7 (IMM resident) but not CypD-Flag (matrix resident) was immunoprecipitated with VDAC1-HA (OMM resident) (Figure S3D, top right). SLC25A30 (IMM resident) and GBAS (OMM resident; Figure S3E) also interacted with VDAC1 (Figure S3D, top right). This reciprocal immunoprecipitation experiment further confirmed that VDAC1 interacts with SPG7. These results suggest that IMM SPG7 may interact directly with CypD, AFG3L2, and VDAC1, while AFG3L2 interacts only with SPG7. We next asked whether SPG7/AFG3L2 association is determinant of SPG7/CypD and SPG7/VDAC1 interaction. To address this, immunoprecipitation was performed in AFG3L2 KD HEK293T cells which were cotransfected with CypD-Flag/SPG7-HA or VDAC1-Flag / SPG7-HA. Immunoprecipitation with HA antibodies were able to pull-down both CypD-Flag and VDAC1-Flag proteins suggesting that SPG7 interaction with CypD and VDAC1 is independent of AFG3L2 interaction (Figure S3F). Collectively, these data establish the formation of a multimeric PTP complex that is composed of OMM, IMM, and matrix components.

Direct Association of SPG7 and CypD in Vivo and in Vitro

To verify that the interaction between SPG7 and CypD occurs in an endogenous condition, HeLa cell lysates were subjected to immunoprecipitation with an antibody specific for SPG7, and immunoprecipitates were probed with an antibody specific for CypD. Similar to ectopic protein-protein interaction data (Figure S3B), binding of endogenous SPG7 and CypD was observed (Figure 3A). The endogenous interaction between SPG7 and CypD was disrupted by CypD inhibitor, CsA, suggesting direct binding of CypD and SPG7 (Figure 3A). As a second test for direct interaction between SPG7 and CypD, we incubated purified SPG7-GST/CypD, AFG3L2-GST/CypD, GST/CypD, or CypD alone. After in vitro binding, glutathione sepharose 4B beads were used to pull-down the complexes. SPG7-GST co-precipitated CypD, while AFG3L2-GST did not pull-down CypD (Figure 3B). GST alone did not interact with CypD suggesting that SPG7 binds directly to CypD.

To determine if the presence of SPG7 alters CypD oligomerization leading to the formation of higher molecular weight complexes, size exclusion chromatography was performed. As a first step, CypD-HA and SPG7-HA were expressed alone and in combination in COS-7 cells (Figure 3C, left). Western blot analysis verified both CypD-HA and SPG7-HA protein expression when probed with an antibody specific for HA. Next, lysates from COS-7 cells

expressing CypD-HA were subjected to size exclusion separation to identify and quantify CypD by molecular weight fraction. As expected, CypD alone eluted around 20 kDa (Figure 3C, first right). Similarly, SPG7 alone eluted as homodimeric or trimeric forms (Figure 3C, second right). Analysis of the eluate fractions by SDS-PAGE revealed coexpressed SPG7 (~89 kDa) and PPIF (~20 kDa) elute at a high molecular weight of ~670 kDa (Figure 3C, third right). Although SPG7 was able to pull-down AFG3L2, we did not observe the CypD-AFG3L2 interaction (Figure 3B and S3B). To further confirm that AFG3L2 and CypD do not form a heterooligomeric complex, lysates from COS-7 cells expressing either AFG3L2-Flag alone or in a combination of AFG3L2-Flag and CypD-Flag were subjected to size exclusion separation to identify and quantify the complex by molecular weight fraction. We found that unlike SGP7, AFG3L2 did not elute in the same fractions as CypD (Figure 3C, bottom right), further supporting the evidence that CypD directly binds SPG7 and not AFG3L2.

To further explore the possibility of direct binding between SPG7 and CypD in a non-mammalian system, a Yeast-2-Hybrid (Y2H) assay was performed (Figure 3D). Fusion proteins of CypD-GAD and full-length SPG7-GBK (FL-SPG7) or truncated SPG7-GBK (t-SPG7) which lacks transmembrane regions were co-transfected in a yeast strain containing a X-α-galactosidase reporter gene (Figure 3E). Since SPG7 is predicted to be a two transmembrane domain (2TM) protein, the truncation mutant lacking the N-terminal transmembrane domain was predictably necessary, because the Y2H interaction occurs in a soluble condition. Western blot analysis confirmed the ectopic expression of both full-length as well as t-SPG7 proteins in yeast (Figure 3F). Yeast containing both the CypD-GAD and t-SPG7-GBK survived on stringent selections and abundant α-gal activity was observed as blue colonies confirming SPG7-CypD interactions, while yeast expressing CypD-GAD, FL-SPG7-GBK, and CypD-GAD + FL-SPG7-GBK failed to thrive (Figure 3G) indicating that SPG7 and CypD can interact in a heterologous system. The CypD-GAD and t-SPG7-GBK expression in the α-gal positive yeast lysate from CypD-GAD + t-SPG7-GBK was confirmed by Western blot analysis (Figure 3H). Taken together, these complementary biochemical results revealed that the interaction of SPG7 and CypD exists as a high molecular weight complex that is CsA sensitive.

Mapping CypD-SPG7 Interaction: C-terminal SPG7 (CID; aa 701–795) Binds CypD

To identify essential regions of SPG7 for CypD binding, we characterized the interaction using two approaches. We first tested a series of C-terminal truncations of SPG7 for their ability to interact with CypD in the mitochondrial matrix (Figure 4A). To identify the interaction between the SPG7 regions and CypD, we expressed these SPG7-FLAG truncation mutants (Δ1, Δ2, Δ3, Δ4, or Δ5) individually or in combination with CypD-HA plasmid constructs in COS-7 cells (Figure 4B, left). Immunoprecipitation of CypD-HA followed by Western blotting revealed that the Δ5 region, corresponding to the C-terminus of SPG7, is determinant of CypD binding (Figure 4B, top right). Since Y2H data revealed that loss of the N-terminal transmembrane regions of SPG7 is not determinant of CypD binding (Figure 3G), we performed protein-protein interaction prediction analysis with a series of soluble C-terminal SPG7 fragment constructs selected for their ability to bind to CypD and induce α-gal activity (Figure 4C). The expression of PPIF-GAD and truncated

SPG7-GBK (t-SPG7), Δ1 t-SPG7, Δ2 t-SPG7, Δ3 t-SPG7 constructs in transformed yeast were verified by Western blot analysis (Figure 4D). Yeast containing both the PPIF and t-SPG7, Δ1 t-SPG7, Δ2 t-SPG7 constructs survived on stringent selection and produced abundant α-gal, while yeast expressing CypD and Δ3 t-SPG7 did not survive (Figure 4E) indicating that SPG7 and CypD interaction is determined by the SPG7 C-terminal region (701–795 aa). Together, these results show that the C-terminus of SPG7, named here as CypD interacting domain (CID) is a determinant of CypD-dependent PTP activity.

SPG7 Proteolytic Activity is Dispensable for PTP Activity

SPG7 was originally characterized as a nuclear-encoded mitochondrial metalloprotease (*m*-AAA), and mutations in SPG7 result in a neurodegenerative disorder, hereditary spastic paraplegia (HSP) (Casari et al., 1998). The SPG7 protease activity maintains protein quality control in the IMM mitochondrial membrane compartment (Nolden et al., 2005; Rugarli and Langer, 2006). Since our biochemical and functional data indicated a role for PTP function, we next examined whether SPG7 proteolytic activity is necessary for CypD interaction and $[Ca^{2+}]_m$ retention. Because SPG7 is a metalloprotease, we generated two SPG7 Zn^{2+} binding domain (proteolytic center) mutant constructs, a disease-associated mutation (G577S; Mut1) and Zn^{2+} binding conserved amino acid triple mutation (H574G, E575G, G577S; Mut2) (Figure 4F and 4I and Figure S4). To investigate whether protease function is necessary for interaction between SPG7 and CypD, Y2H assay was performed. In the Y2H assay, both SPG7 mutants exhibited interaction with CypD (Figure 4G and 4H). To further explore the interaction between the CypD and SPG7 mutants, COS-7 cells were cotransfected with PPIF-HA/SPG7-Flag, PPIF-HA/SPG7^{G577A}-Flag (Mut1) or PPIF-HA/SPG7$^{H574G,\ E574G,\ G577A}$-Flag (Mut2) and immunoprecipitated with HA antibodies (Figure 4I and 4J). Flag-tagged, full-length, Mut1 and Mut2 SPG7 were detected in the immunoprecipitates of CypD-HA suggesting that the proteolytic function of SPG7 is not required for SPG7/CypD binding (Figure 4J). We next investigated whether the loss of function proteolytic mutation increased $[Ca^{2+}]_m$ retention. Wild-type 293T cells stably expressing SPG7 Mut2 were permeabilized and subjected to Ca^{2+} pulses (Figure 4K). Cells expressing SPG7 Mut2 protein were unable to enhance $[Ca^{2+}]_m$ retention indicating that the functional proteolytic domain is not essential for the SPG7 role in PTP activity.

Interaction of CypD, SPG7 and VDAC1 Forms PTP Complex at the OMM and IMM Contact Site

Having observed CsA-sensitive interaction between SPG7 and CypD in an endogenous system, to further analyze whether the interaction between SPG7 and CypD is inhibited by CsA, we ectopically expressed Flag-tagged SPG7 with HA-tagged PPIF in COS-7 cells and immunoprecipitated with or without CsA using anti-HA antibodies. SPG7/CypD interaction was significantly reduced by CsA (Figure 5A). CsA binding residues of CypD (R97G, S101A, Q105A, G114V, N144G, I159H, and W163G) are highly conserved among species (Figure S5A), and therefore to further establish that the CsA binding site is determinant of SPG7 binding, we systematically substituted these seven residues, and protein-protein interaction and $[Ca^{2+}]_m$ retention were examined. Immunoprecipitation of SPG7-HA pulled-down wild-type CypD but not CypD-ΔCsA which revealed that the CsA binding region is determinant of SPG7 binding in the mitochondrial matrix (Figure 5B). As expected size

exclusion analysis revealed that SPG7 and CypD-ΔCsA failed to form heterooligomeric complexes (Figure 5C, bottom). We next examined whether CypD-ΔCsA overexpression increased $[Ca^{2+}]_m$ retention. Wild-type HEK293T cells stably expressing CypD-ΔCsA were permeabilized and subjected to Ca^{2+} pulses (Figure S5B and Figure 5D and 5E) which showed enhanced $[Ca^{2+}]_m$ retention indicating that the CypD-ΔCsA domain is essential for the PTP activity and that CypD may function as an oligomer. To explore the possibility of CypD oligomerization, we designed a protein-protein interaction assay using CypD-HA and CypD-ΔCsA-Flag constructs in COS-7 cells. Co-immunoprecipitation of CypD-HA with HA antibody was able to pull-down CypD-ΔCsA-Flag suggesting that CypD and CypD-ΔCsA form oligomeric complexes though the latter lacks CsA binding property (Figure S5C). Because expression of PPIF-ΔCsA in wild-type cells increased $[Ca^{2+}]_m$ retention capacity (Figure 5D and Figure 5E), it is plausible that oligomerization of CypD determines SPG7 interaction. Therefore to determine if CypD regulation of SPG7 is dependent upon the CsA binding site, 293T cells expressing CypD-ΔCsA-Flag were subjected to immunoprecipitation with an antibody specific for SPG7. As expected, an antibody specific for SPG7 was able to pull-down endogenous CypD in control but was markedly decreased in CypD-ΔCsA indicating that CypD-ΔCsA is a determinant of SPG7 binding (Figure S5D).

Because the PTP is postulated as a multimeric protein complex comprised of both IMM and OMM components (Figure S3) (Kroemer et al., 2007), we hypothesized that the intermembrane space (IMS) region of SPG7 binds to VDAC1. To test this, a series of SPG7 IMS mutations were generated based on protein-protein interaction prediction using ISIS method of PredictProtein. Flag-tagged SPG7 IMS mutant plasmid constructs (ΔS1, ΔS2, or ΔS3,) were cotransfected with HA-tagged full-length VDAC1 in COS-7 cells (Figure 5F). Following immunoprecipitation with an antibody specific for HA, samples were probed with Flag antibody. While full-length SPG7 (FL-SPG7) and ΔS2-SPG7 showed strong interaction with VDAC1, ΔS1 and ΔS3 failed to bind VDAC1, suggesting that the ΔS1 and ΔS3 regions of SPG7, corresponding to the IMS region, are determinant of interaction with VDAC1 (Figure 5G). Because VDAC1-SPG7-CypD form the Ca^{2+}-induced PTP, we next examined whether SPG7 and VDAC1 FPLC profiling was consistent with SPG7 and VDAC1 forming a complex (Figure 5H, bottom) independently of SPG7/CypD. To address this, immunoprecipitation was performed in PPIF KD cells as well as with CsA pretreated HEK293T cells. Immunoprecipitation with HA antibodies was able to pull-down VDAC1-Flag proteins suggesting that SPG7 interaction with VDAC1 is not dependent upon CypD interaction (Figure S5E). We also examined the $[Ca^{2+}]_m$ retention capacity in HEK293T cells expressing either full-length SPG7 (FL-SPG7) or ΔS1-SPG7 and ΔS2-SPG7 (Figure 5I). We found that ΔS1-SPG7 but not FL-SPG7 or ΔS2-SPG7 mutant exhibited increased $[Ca^{2+}]_m$ retention capacity (Figure 5J–5L). Together, these results indicate that the matrix and IMS regions of SPG7 are required for CypD and VDAC1 interactions that assemble the mitochondrial PTP complex.

SPG7 and CypD are Required for Ca^{2+} Overload and ROS-Induced PTP Opening, Mitochondrial Dysfunction, and Cell Death

The MPT is induced following $[Ca^{2+}]_m$ accumulation and ROS overproduction (Crompton, 1999). Since CsA-sensitivity is PPIF dependent, we next explored whether CsA sensitivity

occurs in SPG7 KD mitochondria. When permeabilized 293T Neg shRNA cells were pretreated with CsA (5 μM) and then exposed to Ca^{2+} pulses, augmented CsA-dependent $[Ca^{2+}]_m$ retention was observed (Figure 6A). Remarkably, CsA-dependent $[Ca^{2+}]_m$ retention was similar in both SPG7 KD and PPIF KD without or with CsA pretreatment (Figure 6B and 6C). To ascertain whether mitochondrial integrity was maintained following long duration of Ca^{2+} pulsing, we monitored the $\Delta\Psi_m$ and Ca^{2+} handling in SPG7 and PPIF KD cells without or with Ru360 (Shanmughapriya et al., 2015). Since mitochondrial Ca^{2+} overload is mediated by the MCU complex, following boluses of Ca^{2+} pulses, we delivered Ru360 which blocks the MCU-dependent Ca^{2+} uptake (Figure 6D–6F). Our results indicated that SPG7 KD or PPIF KD $\Delta\Psi_m$ was immediately restored through inhibition of MCU-mediated Ca^{2+} influx demonstrating that the OMM is intact. Importantly, knockdown of either SPG7 or PPIF did not alter mitochondrial Ca^{2+} flux components (Figure S6A–S6C), however SPG7 KD demonstrated enhanced mitochondrial bioenergetics ($NADH/NAD^+$ ratio, ATP and oxygen consumption rate; OCR) (Figure S6D–S6I). To test whether the normalization of OCR abrogated PTP inhibition in SPG7 KD, cells were challenged with antimycin A (5 nM) for 30 minutes. OCR measurements revealed that both basal and maximal OCR were similar to Neg shRNA (Figure S6J–6L). After normalization of bioenergetics, we next investigated the $[Ca^{2+}]_m$ retention in SPG7 KD cells. These results revealed that normalization of bioenergetics in SPG7 KD cells did not alter $[Ca^{2+}]_m$ retention (Figure S6M and S6N) suggesting that SPG7 participates in the PTP complex.

To further investigate the role of SPG7 in PTP opening and mitochondrial dysfunction, we tested mitochondrial swelling as an indicator of PTP opening. Mitochondria isolated from Neg shRNA, SPG7 KD, and PPIF KD HeLa cells were subjected to mitochondrial swelling/permeability transition induction by Ca^{2+} and/or t-butyl hydroperoxide. Mitochondria from SPG7 and PPIF KD cells were resistant to both Ca^{2+} and/or t-butyl hydroperoxide-induced swelling, indicating that SPG7 and CypD are necessary for PTP opening (Figure 6G–6I). Because opening of the PTP uncouples the electron transport chain, leading to dissipation of the $\Delta\Psi_m$ across the IMM, we tested whether Ca^{2+} or H_2O_2-induced PTP opening and $\Delta\Psi_m$ loss are SPG7-dependent in intact cells. To assess the role of SPG7 in Ca^{2+} overload and ROS-induced $\Delta\Psi_m$ dissipation, we used cationic indicator, tetramethylrhodamine ethyl ester (TMRE), which accumulates in healthy mitochondria, and upon $\Delta\Psi_m$ dissipation, mitochondrial-localized TMRE is rapidly lost. Neg shRNA HeLa cells exposed to both ionomycin and H_2O_2 exhibited a significant loss of $\Delta\Psi_m$ (Figure 6J and 6K). In contrast, $\Delta\Psi_m$ was unaffected after exposure to ionomycin and H_2O_2 in SPG7 KD and PPIF KD cells (Figure 6J and 6K). The oxidant and Ca^{2+} overload-induced $\Delta\Psi_m$ dissipation was CsA-sensitive as CsA pretreatment significantly prevented this event (Figure 6J and 6K). To further support these results, we examined PTP opening in intact cells using confocal calcein quenching analysis in which upon PTP opening, mitochondrial calcein fluorescence becomes quenched by cobalt chloride ($CoCl_2$) entering the matrix. Neg shRNA cells treated with ionomycin or H_2O_2 were unable to sustain calcein fluorescence in the mitochondria, while calcein quenching was significantly inhibited in cells lacking SPG7 and CypD (Figure 6L and 6M). Taken together, these findings reveal that SPG7 is an essential component of the PTP complex that promotes Ca^{2+}- and ROS-induced PTP opening.

Although mitochondria play a central role in apoptosis through OMM permeabilization and subsequent release of intermembrane space apoptogens (Tait and Green, 2010), Ca^{2+} overload and ROS-induced necrosis that result from PTP opening are independent of OMM permeabilization. To further confirm the significance of SPG7 and CypD in Ca^{2+}-overload and ROS-induced necrosis, HeLa Neg shRNA, SPG7KD, and PPIF KD mitochondria were treated with Ca^{2+} (200 μM) or pro-apoptotic protein, tBid (truncated Bid; 10 nM), for 10 minutes. Both mitochondrial pellet and the supernatant were evaluated for cytochrome *c* release by Western blot analysis. Cytochrome *c* release from the tBid permeated mitochondria were similar in Neg shRNA, SPG7 KD, and PPIF KD cells but was prevented in $Bax^{-/-}Bak^{-/-}$ double knockout MEFs (Figure S7A). These results revealed that both SPG7 and CypD are not involved in tBid-induced Bax/Bak-dependent OMM permeabilization. To further support the role of SPG7 in Ca^{2+} overload and ROS-induced cell death, cells were exposed to ionomycin (25 μM) or H_2O_2 (0.8 mM) in the absence or presence of CsA (5 μM) for 6 hrs. Consistent with the preservation of mitochondrial function (Figure S6 and Figure 6D–M), ATP levels were significantly decreased in Neg shRNA but not in SPG7 or PPIF KD cells (Figure S7B). We also examined whether SPG7 and PPIF KD cells were resistant to cell death following ionomycin or H_2O_2 challenge. In support, necrotic cell death occurred only in the Neg shRNA cells but not in the SPG7 KD and PPIF KD cells (Figure S7C and S7D). Analysis of necrotic cells indicated that both ionomycin and H_2O_2-mediated cell death are CsA sensitive (Figure S7D).

To further support the role of SPG7 in PTP complex formation and oxidative-stress-induced cell death, we used primary neonatal rat ventricular cardiomyocytes (NRVMs). To verify loss of PTP function, NRVMs were transfected with siRNAs for SPG7 and PPIF and mRNA and protein abundance were measured (Figure S7E–S7G). After RNAi-mediated knockdown, permeabilized NRVMs were analyzed for $[Ca^{2+}]_m$ retention. Consistent with 293T and HeLa cells, increased $[Ca^{2+}]_m$ retention was observed in SPG7 and PPIF knockdown NRVMs (Figure S7H–7J). We next tested whether knockdown of SPG7 prevents Ca^{2+} overload and oxidative stress-induced mitochondrial PTP opening and cell death. Similar to HeLa cells, calcein quenching was seen in scrambled siRNA but not in SPG7 or PPIF KD NRVMs (Figure S7K and S7L). Since SPG7 and PPIF KD NRVMs exhibited reduced PTP opening, possible mitigation of ionomycin and H_2O_2-induced cell death was examined. Control siRNA NRVMs treated with ionomycin or H_2O_2 exhibited marked cell death (Figure S7M and S7N), however knockdown of SPG7 and PPIF significantly prevented ionomycin or H_2O_2-induced cell death (Figure S7M and S7N).

Finally, to confirm the SPG7 role as a PTP component, SPG7 KO 293T cells were generated by CRISPR-Cas9 mediated gene targeting (Figure 7A, and 7B). Similar to shRNA knockdown cells, SPG7 KO 293T cells robustly handled numerous Ca^{2+} pulses with sustained $\Delta\Psi_m$ (Figure 7C and 7D). To further confirm the role of SPG7 as a PTP component, proteolytic dead mutant SPG7 (SPG7 Mut2) was reconstituted in SPG7 KO cells (Figure 7E). Stable expression of SPG7 Mut2 in SPG7 KO cells rescued the PTP phenotype indicating that proteolytic activity is dispensable for PTP activity (Figure 7F). Similar to SPG7 KD cells, SPG7 KO 293T cells were resistant to both ionomycin and H_2O_2-

mediated cell death (Figure 7G). Together, these results demonstrate the role of SPG7 in mitochondrial Ca^{2+} retention, PTP opening, and cell death.

DISUCSSION

Biochemical and genetic studies revealed that PTP opening is dependent on the mitochondrial matrix resident protein CypD (Baines et al., 2005; Basso et al., 2005; Nakagawa et al., 2005; Schinzel et al., 2005; Tanveer et al., 1996). Loss of CypD exhibited enhanced $[Ca^{2+}]_m$ retention and protection from Ca^{2+} and ROS-induced mitochondrial dysfunction and necrosis. On the basis of these evidences, we conducted both functional and physical interaction studies which further confirmed that CypD is necessary for Ca^{2+} and ROS-induced PTP opening. Our protein-protein interaction studies revealed that CypD directly interacts with SPG7, and not the previously proposed PTP components, VDAC1 and ANT2 (Vaseva et al., 2012).

Prior to these findings, SPG7 was described as a mitochondrial AAA protease that forms heterooligomers with a structurally similar metalloprotease, AFG3L2, that is also responsible for assembling ribosomes and eliminating non-functional proteins in the mitochondria (Koppen et al., 2007). When SPG7 is mutated, improper m-AAA protease complex formation results in defective protein quality control, impaired mitochondrial function, and diminished nerve cell signaling causing a challenging human disease, spastic paraplegia (Rugarli and Langer, 2006). However, AFG3L2 alone has been demonstrated sufficient for metalloprotease function by forming homo-oligomers or alternative hetero-oligomers (Koppen et al., 2007). By choosing non-neuronal alternative cell types and a knockdown approach, we were able to separate SPG7's known role as a protease to examine the participation of SPG7 in PTP opening. In fact, throughout our experiments, loss of SPG7 yielded mitochondrial performance that could best be described as enhanced and robust (Figure S6). Additionally, the dual roles of SPG7, that of the metalloprotease and as a PTP component were shown to be independent as loss of heteromeric complex partner, AFG3L2 KD shows less $[Ca^{2+}]_m$ retention than SPG7 KD cells (Figure 1). Hence, while AFG3L2 withstood 16 extramitochondrial Ca^{2+} pulses, the observation that SPG7 KD cells handled ~22 Ca^{2+} pulses was likely attributable to SPG7's previously undescribed PTP function.

While the interactions of SPG7/CypD, SPG7/AFG3L2, SPG7/VDAC1, and VDAC1/GBAS suggest the existence of a PTP supercomplex, we hypothesize that only two interactions (SPG7/CypD and SPG7/VDAC1) are likely to be relevant to PTP opening. Our data strongly support SPG7 and CypD forming a complex between the IMM and matrix. However, overexpression of SPG7 in control cells did not increase mitochondria susceptibility to Ca^{2+}-induced PTP opening (unpublished observation). Additionally, VDAC1 interaction with SPG7 is likely important as VDAC's non-selective channel function at the OMM would greatly influence IMM PTP opening, because VDACs are the main non-selective proteins critical for transporting ions and solutes across the OMM (Colombini, 2012; Hiller et al., 2008). Surprisingly, VDAC1 associated with SPG7 and demonstrated protection from mitochondrial Ca^{2+} overload (Figure 1 and Figure S3). It is also consistent with previous studies that CypD does not interact directly with VDAC1 or

ANT (Vaseva et al., 2012), however VDAC1 is a component of a CypD/SPG7/VDAC1 PTP complex.

Three VDAC isoforms exist in mammals, and many previous studies have focused on this OMM non-selective anion channel in the context of cell death. VDAC1/VDAC3 knockout mice are viable, but mitochondrial functional abnormalities were observed (Anflous et al., 2001). Intriguingly, deletion of VDAC2 resulted in embryonic lethality, and VDAC2 null cells are hyper-sensitive to intrinsic apoptotic cell death (Cheng et al., 2003). Moreover, Ca^{2+} and ROS-induced PTP-dependent cell death were indistinguishable between wild-type and a combination of double or triple deletion of VDAC isoforms (Baines et al., 2007). Remarkably, double knockout of VDAC1/VDAC3 in mice is associated with learning impairments and deficits in short-and long-term synaptic plasticity (Weeber et al., 2002). Genetic ablation of SPG7 resulted in spasticity of lower limbs, abnormal axons and dendrites which are shorter in length, brisk reflexes, cognitive dysfunction, muscle weakness, and bladder disturbances in aged mice (Ferreirinha et al., 2004). Interestingly, deletion of PPIF did not offer any distinguishable phenotype in young mice (12 weeks) (Baines et al., 2005). However, in aged mice, obesity, behavioral defects and memory impairment were observed (Luvisetto et al., 2008; Mouri et al., 2010). These animals' cumulative neurological phenotypes suggest a physiological role for PTP complex and loss of function could lead to pathological symptoms such as Alzheimer's disease, ischemia and multiple sclerosis. Our findings not only reveal the PTP complex molecular identity but also contribute understanding to physiological role of PTP complex and therapeutic strategy for the degenerative disorders. Although the precise phenotype of PTP is unknown, we speculate that CypD, SPG7, and VDAC1 are core components residing in the matrix, IMM, and OMM, respectively. Since PTP activity is modulated by both Ca^{2+} and ROS, CypD may participate in a Ca^{2+} and ROS-sensitive mechanism, while PTP core components, SPG7 and VDAC1, could be modulated by various signals.

In summary, our cellular, biochemical, and genetic experimental findings suggest the existence of a PTP integral junction in which several proteins determine $[Ca^{2+}]_m$ overload-dependent PTP opening. The mitochondrial IMM and matrix harbor SPG7 and CypD which are essential for PTP opening. SPG7 is a core component of the PTP which not only interacts with matrix protein CypD but also with the OMM channel VDAC1 at OMM/IMM contact sites. Although questions remain, the identification of the PTP complex will permit manipulation of these structures in vitro and in vivo to rigorously investigate SPG7-dependent PTP function in health and disease.

EXPERIMENTAL PROCEDURES

Additional information regarding primary NRVMs, HEK293T, HeLa, and COS-7 cultures, plasmids, buffers, antibodies, primer sequences, sample preparation, cell permeabilization and detailed procedures are provided in the Extended Experimental Procedures.

Primary Cell Isolation and Cell Cultures

HEK293T, HeLa and COS-7 were obtained from ATCC and maintained in Dulbecco's modified Eagle's medium (DMEM) supplemented with 10% FBS, and penicillin/

streptomycin. NRVMs were cultured in Ham's F-10 supplemented with 5% fetal bovine serum (FBS) and penicillin/streptomycin. Details can be found in Extended Experimental Procedures.

Generation of Stable shRNA Knockdown Cell Lines

HEK293T and HeLa (5×10^5 per well) were infected with lentivirus expressing short hairpin RNA (for knockdown experiments). 48 hr post-infection, cells were selected with puromycin (2 μg/ml) for 10 days. Details can be found in Extended Experimental Procedures.

Ca^{2+} Uptake and $\Delta\Psi_m$ Measurement in Permeabilized Cell System

The simultaneous measurement of $\Delta\Psi_m$ and extramitochondrial Ca^{2+} ($[Ca^{2+}]_{out}$) clearance as an indicator of $[Ca^{2+}]_m$ retention was achieved as described previously (Mallilankaraman et al., 2012a; Mallilankaraman et al., 2012b). A series of Ca^{2+} boluses (10 μM) and mitochondrial uncoupler, CCCP (2 μM), were added at the indicated time points.

Size Exclusion Chromatographic Analysis of PTP Complex

Gel filtration was performed at 4°C by fast protein liquid chromatography (ÄKTA Pure FPLC; GE Healthcare), and the Superdex-200 Increase 10/300 GL column was equilibrated with PBS. Column calibration was carried out with a gel filtration protein standards kit (Bio-Rad) (Park et al., 2009). Cell lysates were directly loaded onto the column and fractions were collected at a flow rate of 0.5 ml/min.

Mitochondrial Isolation and Swelling Assay

HeLa cell mitochondria were isolated as described previously (Hoffman et al., 2013). Isolated mitochondria were subjected to swelling assay. Mitochondrial swelling was measured by decrease in absorbance at 540 nm after addition of Ca^{2+} (250 μM) or t-BH (100 μM) (Tecan) (Riley and Pfeiffer, 1985). Details can be found in Extended Experimental Procedures.

NADH/NAD^+ Measurement

Neg shRNA, SPG7 and PPIF KD 293T cells were transiently transfected with NADH-NAD^+ redox sensor, peredox m-cherry (Hung et al., 2011). Confocal images were acquired at 405 nm and 561 nm excitation every 3s using Carl Zeiss 710 Meta NLO.

Statistical Analyses

Data from multiple experiments were quantified and expressed as Mean ± SE., and differences between groups were analyzed by using two-tailed paired Student's t-test or, when not normally distributed, a nonparametric Mann-Whitney *U* test. Differences in means among multiple data sets were analyzed using 1-way ANOVA with the Kruskal-Wallis test, followed by pairwise comparison using the Dunn test. *P* value less than 0.05 was considered significant in all analysis. The data were computed either with Graphpad Prism version 6.0 or SigmaPlot 11.0 Software.

Supplementary Material

Refer to Web version on PubMed Central for supplementary material.

ACKNOWLEDGMENTS

We thank Craig B. Thompson, Alexander M. van der Bliek, and Gary Yellen for sharing $Bax^{-/-}Bak^{-/-}$ MEFs, Drp1 plasmid constructs, Peredox plasmid construct, respectively. This research was funded by the National Institutes of Health (R01GM109882, R01HL086699, R01HL119306, and 1S10RR027327 to MM).

REFERENCES

Alavian KN, Beutner G, Lazrove E, Sacchetti S, Park HA, Licznerski P, Li H, Nabili P, Hockensmith K, Graham M, et al. An uncoupling channel within the c-subunit ring of the F1FO ATP synthase is the mitochondrial permeability transition pore. Proc Natl Acad Sci U S A. 2014; 111:10580–10585. [PubMed: 24979777]

Anflous K, Armstrong DD, Craigen WJ. Altered mitochondrial sensitivity for ADP and maintenance of creatine-stimulated respiration in oxidative striated muscles from VDAC1-deficient mice. J Biol Chem. 2001; 276:1954–1960. [PubMed: 11044447]

Atorino L, Silvestri L, Koppen M, Cassina L, Ballabio A, Marconi R, Langer T, Casari G. Loss of m-AAA protease in mitochondria causes complex I deficiency and increased sensitivity to oxidative stress in hereditary spastic paraplegia. J Cell Biol. 2003; 163:777–787. [PubMed: 14623864]

Baines CP, Kaiser RA, Purcell NH, Blair NS, Osinska H, Hambleton MA, Brunskill EW, Sayen MR, Gottlieb RA, Dorn GW, et al. Loss of cyclophilin D reveals a critical role for mitochondrial permeability transition in cell death. Nature. 2005; 434:658–662. [PubMed: 15800627]

Baines CP, Kaiser RA, Sheiko T, Craigen WJ, Molkentin JD. Voltage-dependent anion channels are dispensable for mitochondrial-dependent cell death. Nat Cell Biol. 2007; 9:550–555. [PubMed: 17417626]

Basso E, Fante L, Fowlkes J, Petronilli V, Forte MA, Bernardi P. Properties of the permeability transition pore in mitochondria devoid of Cyclophilin D. J Biol Chem. 2005; 280:18558–18561. [PubMed: 15792954]

Bernardi P. Mitochondrial transport of cations: channels, exchangers, and permeability transition. Physiol Rev. 1999; 79:1127–1155. [PubMed: 10508231]

Bonora M, Bononi A, De Marchi E, Giorgi C, Lebiedzinska M, Marchi S, Patergnani S, Rimessi A, Suski JM, Wojtala A, et al. Role of the c subunit of the FO ATP synthase in mitochondrial permeability transition. Cell cycle. 2013; 12:674–683. [PubMed: 23343770]

Casari G, De Fusco M, Ciarmatori S, Zeviani M, Mora M, Fernandez P, De Michele G, Filla A, Cocozza S, Marconi R, et al. Spastic paraplegia and OXPHOS impairment caused by mutations in paraplegin, a nuclear-encoded mitochondrial metalloprotease. Cell. 1998; 93:973–983. [PubMed: 9635427]

Cereghetti GM, Stangherlin A, Martins de Brito O, Chang CR, Blackstone C, Bernardi P, Scorrano L. Dephosphorylation by calcineurin regulates translocation of Drp1 to mitochondria. Proc Natl Acad Sci U S A. 2008; 105:15803–15808. [PubMed: 18838687]

Cheng EH, Sheiko TV, Fisher JK, Craigen WJ, Korsmeyer SJ. VDAC2 inhibits BAK activation and mitochondrial apoptosis. Science. 2003; 301:513–517. [PubMed: 12881569]

Colombini M. VDAC structure, selectivity, and dynamics. Biochim Biophys Acta. 2012; 1818:1457–1465. [PubMed: 22240010]

Crompton M. The mitochondrial permeability transition pore and its role in cell death. Biochem J. 1999; 341(Pt 2):233–249. [PubMed: 10393078]

Duchen MR. Mitochondria and calcium: from cell signalling to cell death. J Physiol. 2000; 52(Pt 1): 57–68. [PubMed: 11080251]

Elrod JW, Wong R, Mishra S, Vagnozzi RJ, Sakthievel B, Goonasekera SA, Karch J, Gabel S, Farber J, Force T, et al. Cyclophilin D controls mitochondrial pore-dependent Ca(2+) exchange,

metabolic flexibility, and propensity for heart failure in mice. J Clin Invest. 2010; 120:3680–3687. [PubMed: 20890047]

Ferreirinha F, Quattrini A, Pirozzi M, Valsecchi V, Dina G, Broccoli V, Auricchio A, Piemonte F, Tozzi G, Gaeta L, et al. Axonal degeneration in paraplegin-deficient mice is associated with abnormal mitochondria and impairment of axonal transport. J Clin Invest. 2004; 113:231–242. [PubMed: 14722615]

Frank S, Gaume B, Bergmann-Leitner ES, Leitner WW, Robert EG, Catez F, Smith CL, Youle RJ. The role of dynamin-related protein 1, a mediator of mitochondrial fission, in apoptosis. Developmental cell. 2001; 1:515–525. [PubMed: 11703942]

Giorgio V, von Stockum S, Antoniel M, Fabbro A, Fogolari F, Forte M, Glick GD, Petronilli V, Zoratti M, Szabo I, et al. Dimers of mitochondrial ATP synthase form the permeability transition pore. Proc Natl Acad Sci U S A. 2013; 110:5887–5892. [PubMed: 23530243]

Halestrap AP. Mitochondrial calcium in health and disease. Biochim Biophys Acta. 2009; 1787:1289–1290. [PubMed: 19695375]

Halestrap AP, Griffiths EJ, Connern CP. Mitochondrial calcium handling and oxidative stress. Biochem Soc Trans. 1993; 21:353–358. [PubMed: 8359495]

Hiller S, Garces RG, Malia TJ, Orekhov VY, Colombini M, Wagner G. Solution structure of the integral human membrane protein VDAC-1 in detergent micelles. Science. 2008; 321:1206–1210. [PubMed: 18755977]

Hoffman NE, Chandramoorthy HC, Shamugapriya S, Zhang X, Rajan S, Mallilankaraman K, Gandhirajan RK, Vagnozzi RJ, Ferrer LM, Sreekrishnanilayam K, et al. MICU1 motifs define mitochondrial calcium uniporter binding and activity. Cell reports. 2013; 5:1576–1588. [PubMed: 24332854]

Hung YP, Albeck JG, Tantama M, Yellen G. Imaging cytosolic NADH-NAD(+) redox state with a genetically encoded fluorescent biosensor. Cell Metab. 2011; 14:545–554. [PubMed: 21982714]

Ichas F, Jouaville LS, Mazat JP. Mitochondria are excitable organelles capable of generating and conveying electrical and calcium signals. Cell. 1997; 89:1145–1153. [PubMed: 9215636]

Koppen M, Metodiev MD, Casari G, Rugarli EI, Langer T. Variable and tissue-specific subunit composition of mitochondrial m-AAA protease complexes linked to hereditary spastic paraplegia. Mol Cell Biol. 2007; 27:758–767. [PubMed: 17101804]

Kroemer G, Galluzzi L, Brenner C. Mitochondrial membrane permeabilization in cell death. Physiol Rev. 2007; 87:99–163. [PubMed: 17237344]

Luvisetto S, Basso E, Petronilli V, Bernardi P, Forte M. Enhancement of anxiety, facilitation of avoidance behavior, and occurrence of adult-onset obesity in mice lacking mitochondrial cyclophilin D. Neuroscience. 2008; 155:585–596. [PubMed: 18621101]

Mallilankaraman K, Cardenas C, Doonan PJ, Chandramoorthy HC, Irrinki KM, Golenar T, Csordas G, Madireddi P, Yang J, Muller M, et al. MCUR1 is an essential component of mitochondrial Ca2+ uptake that regulates cellular metabolism. Nat Cell Biol. 2012a; 14:1336–1343. [PubMed: 23178883]

Mallilankaraman K, Doonan P, Cardenas C, Chandramoorthy HC, Muller M, Miller R, Hoffman NE, Gandhirajan RK, Molgo J, Birnbaum MJ, et al. MICU1 is an essential gatekeeper for MCU-mediated mitochondrial Ca(2+) uptake that regulates cell survival. Cell. 2012b; 151:630–644. [PubMed: 23101630]

Mouri A, Noda Y, Shimizu S, Tsujimoto Y, Nabeshima T. The role of cyclophilin D in learning and memory. Hippocampus. 2010; 20:293–304. [PubMed: 19437409]

Nakagawa T, Shimizu S, Watanabe T, Yamaguchi O, Otsu K, Yamagata H, Inohara H, Kubo T, Tsujimoto Y. Cyclophilin D-dependent mitochondrial permeability transition regulates some necrotic but not apoptotic cell death. Nature. 2005; 434:652–658. [PubMed: 15800626]

Newmeyer DD, Ferguson-Miller S. Mitochondria: releasing power for life and unleashing the machineries of death. Cell. 2003; 112:481–490. [PubMed: 12600312]

Nolden M, Ehses S, Koppen M, Bernacchia A, Rugarli EI, Langer T. The m-AAA protease defective in hereditary spastic paraplegia controls ribosome assembly in mitochondria. Cell. 2005; 123:277–289. [PubMed: 16239145]

Pagliarini DJ, Calvo SE, Chang B, Sheth SA, Vafai SB, Ong SE, Walford GA, Sugiana C, Boneh A, Chen WK, et al. A mitochondrial protein compendium elucidates complex I disease biology. Cell. 2008; 134:112–123. [PubMed: 18614015]

Park CY, Hoover PJ, Mullins FM, Bachhawat P, Covington ED, Raunser S, Walz T, Garcia KC, Dolmetsch RE, Lewis RS. STIM1 clusters and activates CRAC channels via direct binding of a cytosolic domain to Orai1. Cell. 2009; 136:876–890. [PubMed: 19249086]

Riley WW Jr, Pfeiffer DR. Relationships between Ca2+ release, Ca2+ cycling, and Ca2+-mediated permeability changes in mitochondria. J Biol Chem. 1985; 260:12416–12425. [PubMed: 2413023]

Rugarli EI, Langer T. Translating m-AAA protease function in mitochondria to hereditary spastic paraplegia. Trends Mol Med. 2006; 12:262–269. [PubMed: 16647881]

Schinzel AC, Takeuchi O, Huang Z, Fisher JK, Zhou Z, Rubens J, Hetz C, Danial NN, Moskowitz MA, Korsmeyer SJ. Cyclophilin D is a component of mitochondrial permeability transition and mediates neuronal cell death after focal cerebral ischemia. Proc Natl Acad Sci U S A. 2005; 102:12005–12010. [PubMed: 16103352]

Shanmughapriya S, Rajan S, Hoffman NE, Zhang X, Guo S, Kolesar JE, Hines KJ, Ragheb J, Jog NR, Caricchio R, et al. Ca2+ signals regulate mitochondrial metabolism by stimulating CREB-mediated expression of the mitochondrial Ca2+ uniporter gene MCU. Sci Signal. 2015; 8:ra23. [PubMed: 25737585]

Smirnova E, Griparic L, Shurland DL, van der Bliek AM. Dynamin-related protein Drp1 is required for mitochondrial division in mammalian cells. Mol Biol Cell. 2001; 12:2245–2256. [PubMed: 11514614]

Smith AC, Blackshaw JA, Robinson AJ. MitoMiner: a data warehouse for mitochondrial proteomics data. Nucleic acids research. 2012; 40:D1160–D1167. [PubMed: 22121219]

Tait SW, Green DR. Mitochondria and cell death: outer membrane permeabilization and beyond. Nat Rev Mol Cell Biol. 2010; 11:621–632. [PubMed: 20683470]

Tanveer A, Virji S, Andreeva L, Totty NF, Hsuan JJ, Ward JM, Crompton M. Involvement of cyclophilin D in the activation of a mitochondrial pore by Ca2+ and oxidant stress. European journal of biochemistry / FEBS. 1996; 238:166–172. [PubMed: 8665934]

Vaseva AV, Marchenko ND, Ji K, Tsirka SE, Holzmann S, Moll UM. p53 opens the mitochondrial permeability transition pore to trigger necrosis. Cell. 2012; 149:1536–1548. [PubMed: 22726440]

Weeber EJ, Levy M, Sampson MJ, Anflous K, Armstrong DL, Brown SE, Sweatt JD, Craigen WJ. The role of mitochondrial porins and the permeability transition pore in learning and synaptic plasticity. J Biol Chem. 2002; 277:18891–18897. [PubMed: 11907043]

Williams GS, Boyman L, Chikando AC, Khairallah RJ, Lederer WJ. Mitochondrial calcium uptake. Proc Natl Acad Sci U S A. 2013; 110:10479–10486. [PubMed: 23759742]

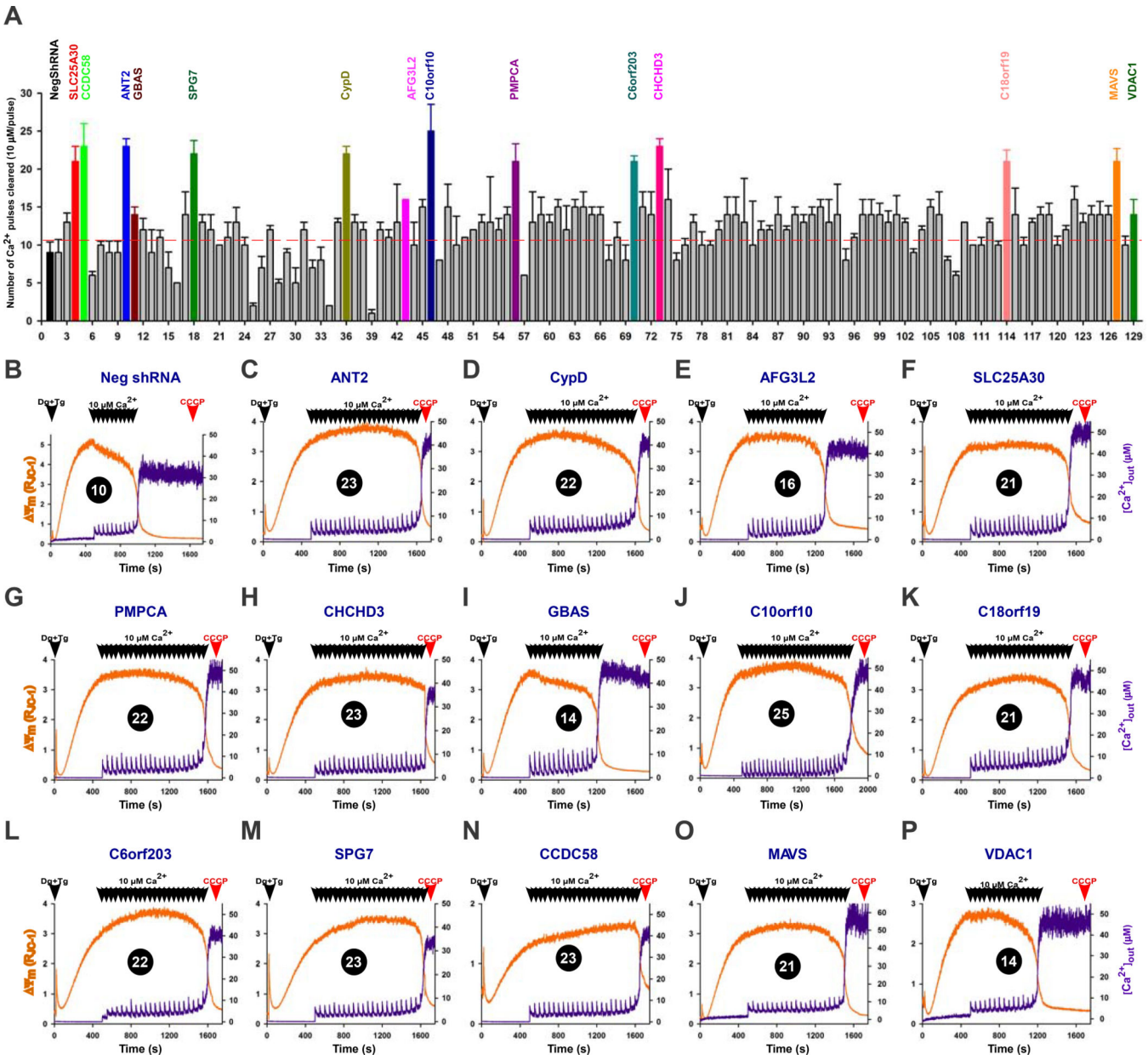

Figure 1. Characterization of the Molecular Identity of Mitochondrial Ca^{2+}-Induced PTP Opening

(A) HEK293T cells stably expressing lentiviral Neg shRNA or shRNA against 128 mitochondrial PTP candidate genes. X-axis numbers represent one PTP candidate knockdown (KD) (see Table S1). Bars represent quantification of the number of $[Ca^{2+}]_{out}$ pulses (10 μM) handled by the mitochondria ($[Ca^{2+}]_m$ retention) before collapsing $\Delta\Psi_m$. Mean ± SEM.; n=3–4. See also Figure S1.

(B) Representative traces of $[Ca^{2+}]_{out}$ clearance (purple) and $\Delta\Psi_m$ (orange). 293T cells stably expressing negative shRNA (control). n=6. See also Figure S1.

(C–P) Representative traces of $[Ca^{2+}]_{out}$ clearance (purple) and $\Delta\Psi_m$ (orange). 293T cells stably knockdown for PTP candidates sequestered between 14–25 Ca^{2+} pulses (10 μM) before $\Delta\Psi_m$ depolarization. n=3–4. See also Figure S1 and Table S1.

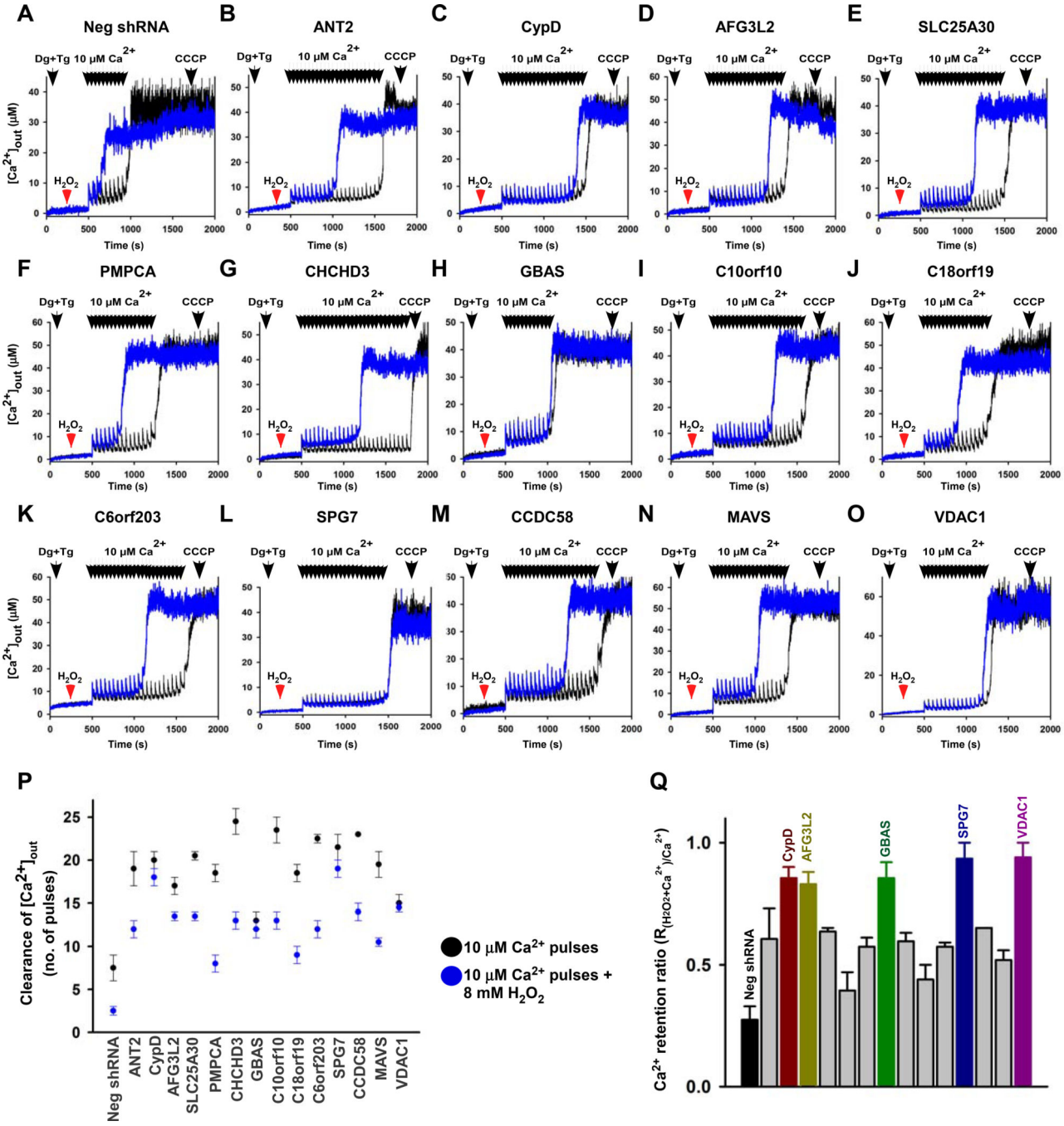

Figure 2. Silencing of SPG7, PPIF, and VDAC1 Prevents Oxidant-Dependent PTP Sensitization

(A–O) Representative traces of $[Ca^{2+}]_{out}$ clearance with or without H_2O_2 (8 mM) pretreatment at 250 seconds. $[Ca^{2+}]_{out}$ pulses and CCCP were delivered as indicated. 293T cells stably expressing Neg shRNA handled nine Ca^{2+} pulses (10 μM) without H_2O_2 pretreatment (black) and three pulses with H_2O_2 pretreatment (blue). A similar protocol was applied for 14 PTP candidates. n=3–4.

(P) Quantification of number of Ca^{2+} pulses handled in PTP candidate 293T KD cells with (blue) or without H_2O_2 (black). Mean ± SEM.; n=3–4.

(Q) Bar graph illustrates $[Ca^{2+}]_m$ retention ratio ($R(H_2O_2+Ca^{2+})/Ca^{2+}$). Mean ± SEM.; n=3–4. See also Figure S2.

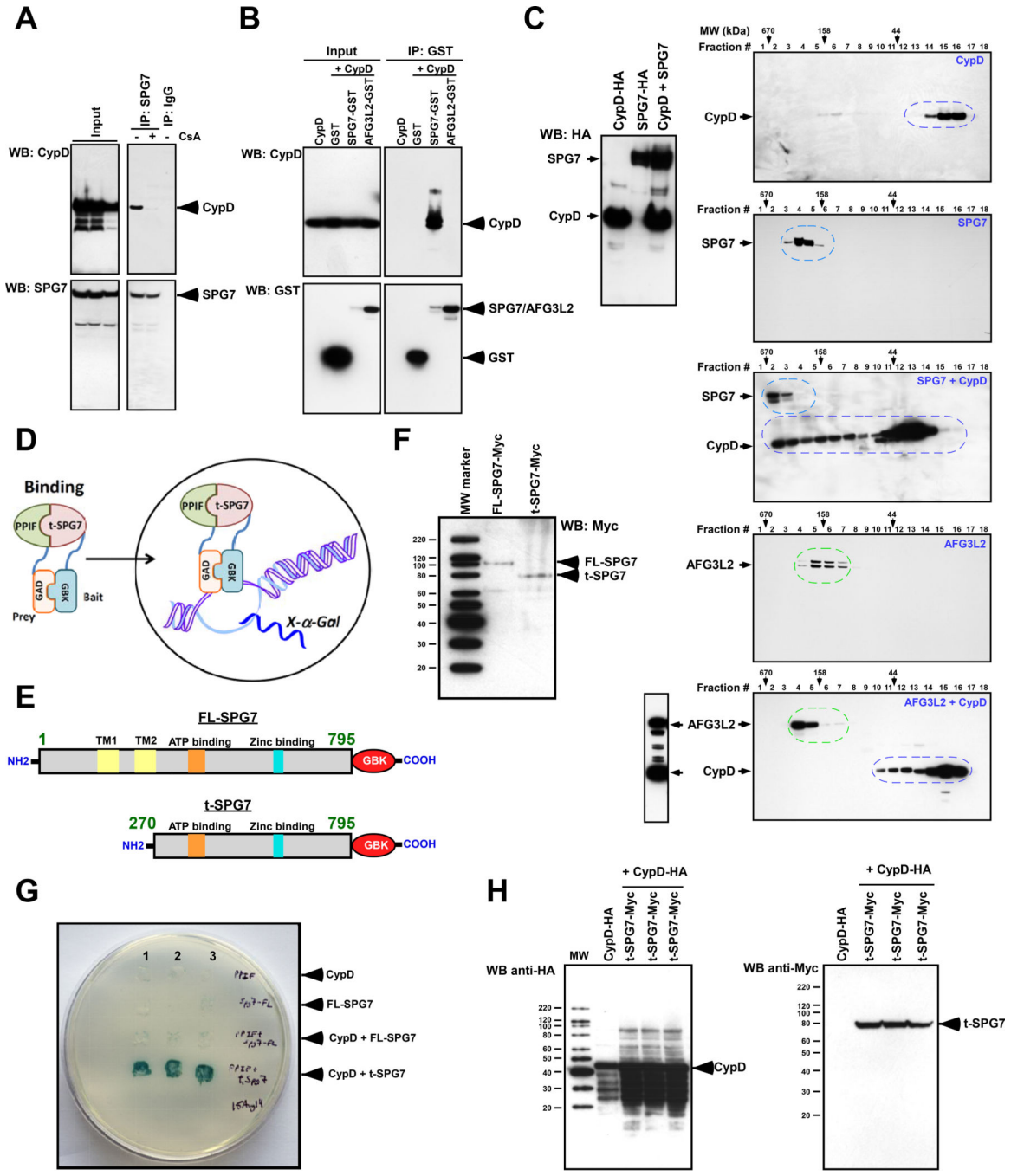

Figure 3. SPG7 Directly Binds CypD

(A) HeLa cell lysate was pretreated with or without CsA (CsA; 5 μM) and immunoprecipitated with SPG7 antibody. IgG was used as a negative control. Inputs (left) and immunoprecipitates (right) were probed with antibodies specific for SPG7 (bottom) and CypD (top). n=5.

(B) Western blot analysis of GST-pull down assays performed using purified CypD and GST, SPG7-GST, and AFG3L2-GST. GST protein was used as negative control. Inputs

(left) and glutathione sepharose-4B beads pull-down samples (right) were probed with antibodies specific for GST (bottom) and CypD (top). n=4.

(C) COS-7 cells expressing CypD-HA, SPG7-HA or CypD-HA and SPG7-HA were lysed, and cell lysates were probed with antibodies specific for HA (left). These cell lysates were separated on a Superdex column, and fractions were immunoblotted with HA antibody (right). COS-7 cells expressing AFG3L2-Flag or AFG3L2-Flag and CypD-Flag were lysed, and cell lysates were fractionated and immunoblotted with Flag antibody. The bottom left panel indicates the coexpression of CypD-Flag and AFG3L2-Flag. n=3.

(D) Schematic of yeast two-hybrid assay for SPG7 and CypD interaction.

(E) Full-length SPG7 with its functional domains (FL-SPG7;top) and truncated SPG7 lacking N-terminal region (t-SPG7-(Δ270 aa); bottom).

(F) Western blot analysis of yeast lysates expressing Myc-tagged Full-length SPG7 (FL-SPG7) and Myc-tagged t-SPG7. n=3.

(G) Full-length SPG7 and t-SPG7 were subcloned into GBK vector as bait, and PPIF was cloned into a GAD vector as prey. Upon interaction, yeast expressing GBK-tSPG7/GAD-CypD activated X-α-gal and produced blue colonies (triplicates). GBK-FL-SPG7, GAD-CypD, pGBK-FL-SPG7/pGAD-CypD were negative for X-α-gal. n=3.

(H) Western blot analysis of lysates prepared from X-α-gal activation-positive t-SPG7+CypD yeast cells in panel G were immunoblotted for HA (left) and Myc (right). n=3. See also Figure S3.

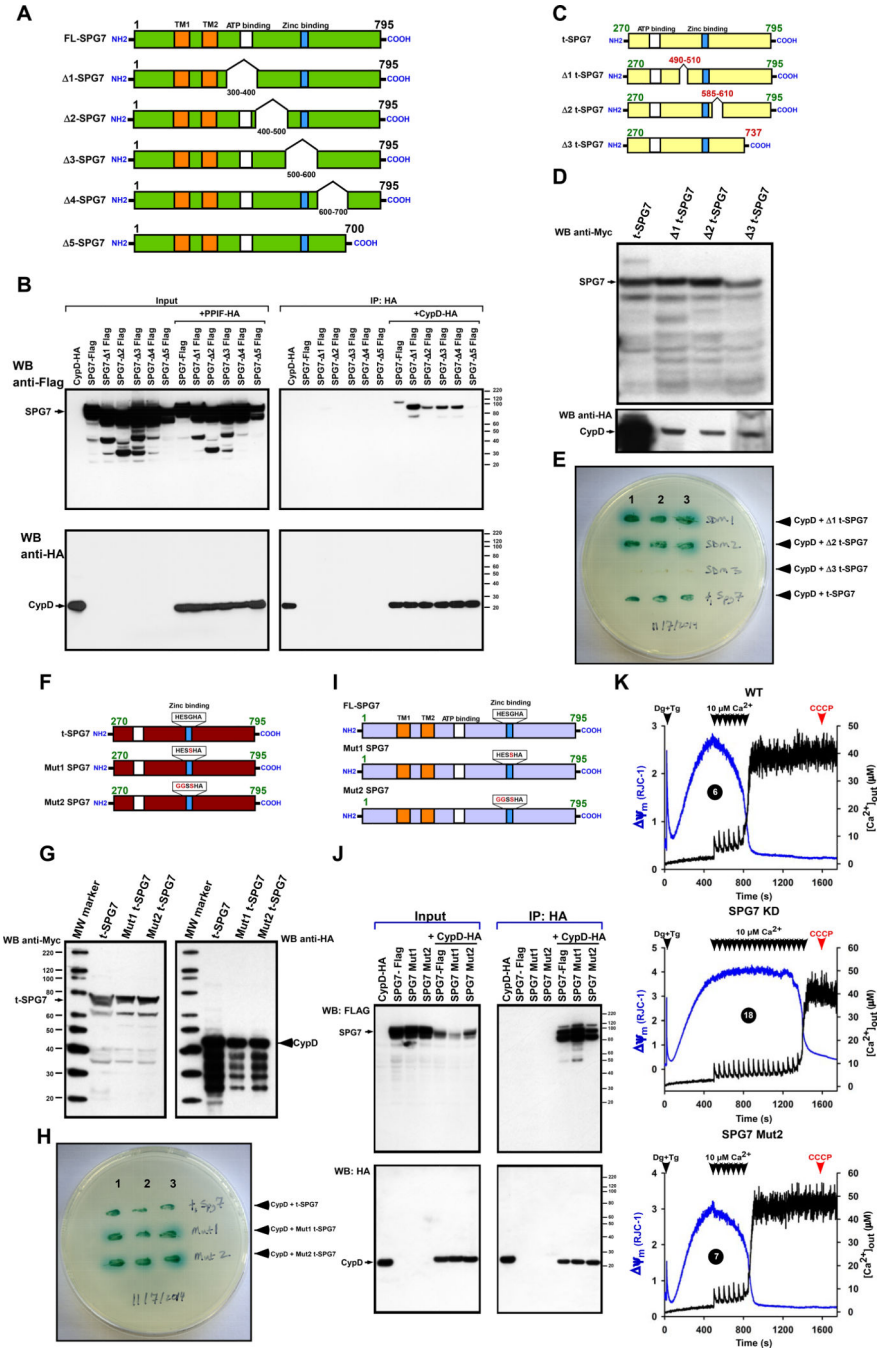

Figure 4. SPG7 C-Terminus Interacts with CypD, and the SPG7 Proteolytic Activity is Dispensable for SPG7-CypD PTP function

(A) Full-length SPG7 with its functional domains (FL-SPG7) and truncated SPG7 (Δ1-Δ5-SPG7).

(B) Cell lysates (left) or immunoprecipitated material (right) from COS-7 cells expressing CypD-HA/SPG7-Flag or CypD-HA/Δ1–5-SPG7-Flag and immunoblotted for Flag (Top) and HA (Bottom). n=3.

(C) t-SPG7 with its functional domains and truncated t-SPG7 (Δ1-Δ3 t-SPG7) for Y2H assay.

(D) Lysates from yeast cells co-expressing CypD-HA/t-SPG7-Myc or CypD-HA/Δ1–3 tSPG7-Myc and immunoblotted for Myc (Top) and HA (Bottom). n=3.
(E) As in Figure 3G, yeast were transformed with GBK-t-SPG7/GAD-PPIF and GBK-Δ1–3t–SPG7/GAD-PPIF and subjected to selection. X-α-gal activation was shown as triplicate blue colonies. GBK-Δ3 t-SPG7/GAD-CypD was negative for X-α-gal. n=3.
(F) t-SPG7 (top) and t-SPG7 proteolytic domain mutants (Mut1 and Mut2 t-SPG7; bottom).
(G) Lysates from yeast cells coexpressing CypD-HA + t-SPG7-Myc, t-SPG7Mut1-Myc, or t-SPG7 Mut2-Myc were immunoblotted for Myc (left) and HA (right). n=3.
(H) As in Figure 3G, yeast were transformed with GBK-t-SPG7/GAD-PPIF, GBK-t-SPG7Mut1/GAD-PPIF and GBK-t-SPG7Mut2/GAD-PPIF and subjected to selection. X-α-gal activation was shown as triplicate blue colonies. n=3.
(I) Full-length SPG7 (top) and proteolytic domain mutants (Mut1 and Mut2 FL-SPG7; bottom).
(J) Cell lysates (left) or immunoprecipitated material (right) from COS-7 cells expressing CypD-HA + FL-SPG7-Flag, SPG7 Mut1-Flag, or SPG7 Mut2-Flag were immunoblotted for Flag (Top) and HA (Bottom). n=4.
(K) Similar to Figure 1B, representative traces of $[Ca^{2+}]_{out}$ clearance (black) and $\Delta\Psi_m$ (blue). 293T wild-type (top), SPG7 KD (middle) or wild-type cells stably expressing SPG7 Mut2 (bottom). n=3. See also Figure S4.

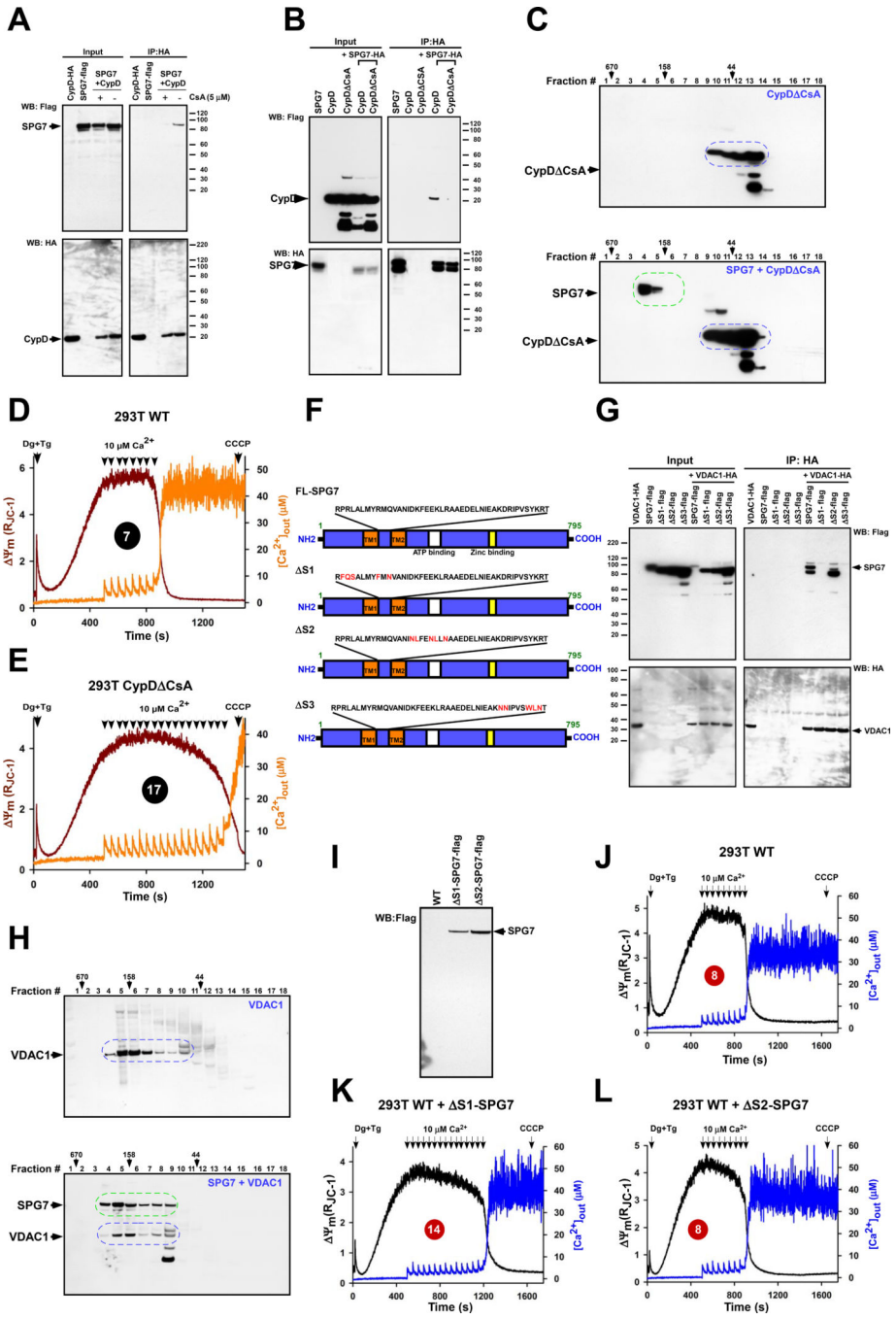

Figure 5. Interaction of CypD, SPG7 and VDAC1 Forms the PTP Complex at OMM and IMM Contact Site

(A) Western blots of cell lysates (left) or immunoprecipitated material (right) from COS-7 cells expressing HA-tagged CypD and/or Flag-tagged SPG7. COS-7 cell lysates were pretreated with CsA (5 μM), immunoprecipitated with HA antibody, and immunoblotted for Flag (top) or HA (bottom). (n = 4).

(B) Western blots of cell lysates (left) or immunoprecipitated material (right) from COS-7 cells expressing HA-tagged SPG7, Flag-CypD wild-type, and Flag-CypD-ΔCsA. HA-immunoprecipitated material was immunoblotted for Flag (top) or HA (bottom). (n = 3).
(C) COS-7 cells expressing CypD-ΔCsA-Flag (top) or CypD-ΔCsA-Flag and SPG7-Flag (bottom) were lysed, gel filtration column fractions were immunoblotted with Flag antibodies. n=3.
(D and E) Similar to Figure 1B, representative traces of $[Ca^{2+}]_{out}$ clearance (orange) and $\Delta\Psi_m$ (brown). 293T wild-type (top) or wild-type cells stably expressing CypD-ΔCSA (bottom). n=3.
(F) Schematic of full-length SPG7 with its functional domains (FL-SPG7). Mutations in FL-SPG7 are highlighted in red (ΔS1, ΔS2, ΔS3).
(G) Western blots of cell lysates (left) or immunoprecipitated material (right) from COS-7 cells expressing SPG7-Flag, VDAC1-HA, and ΔS1-ΔS3-Flag. HA antibody co-immunoprecipitated FL-SPG7-Flag and ΔS2-Flag with VDAC1-HA. n=3.
(H) COS-7 cells expressing VDAC1-HA (top) or coexpressing VDAC1-HA and SPG7-HA (bottom) were lysed, and gel filtration column fractions were immunoblotted with HA antibodies. n=3.
(I) Western blot analysis of 293T wild-type or wild-type cells stably expressing ΔS1-SPG7-Flag and ΔS2-SPG7-Flag.
(J–L) Similar to Figure 1B, representative traces of $[Ca^{2+}]_{out}$ clearance (blue) and $\Delta\Psi_m$ (black). 293T wild-type (J), wild-type cells stably expressing ΔS1-SPG7-Flag (K) or ΔS2-SPG7-Flag (K). n=3. See also Figure S5.

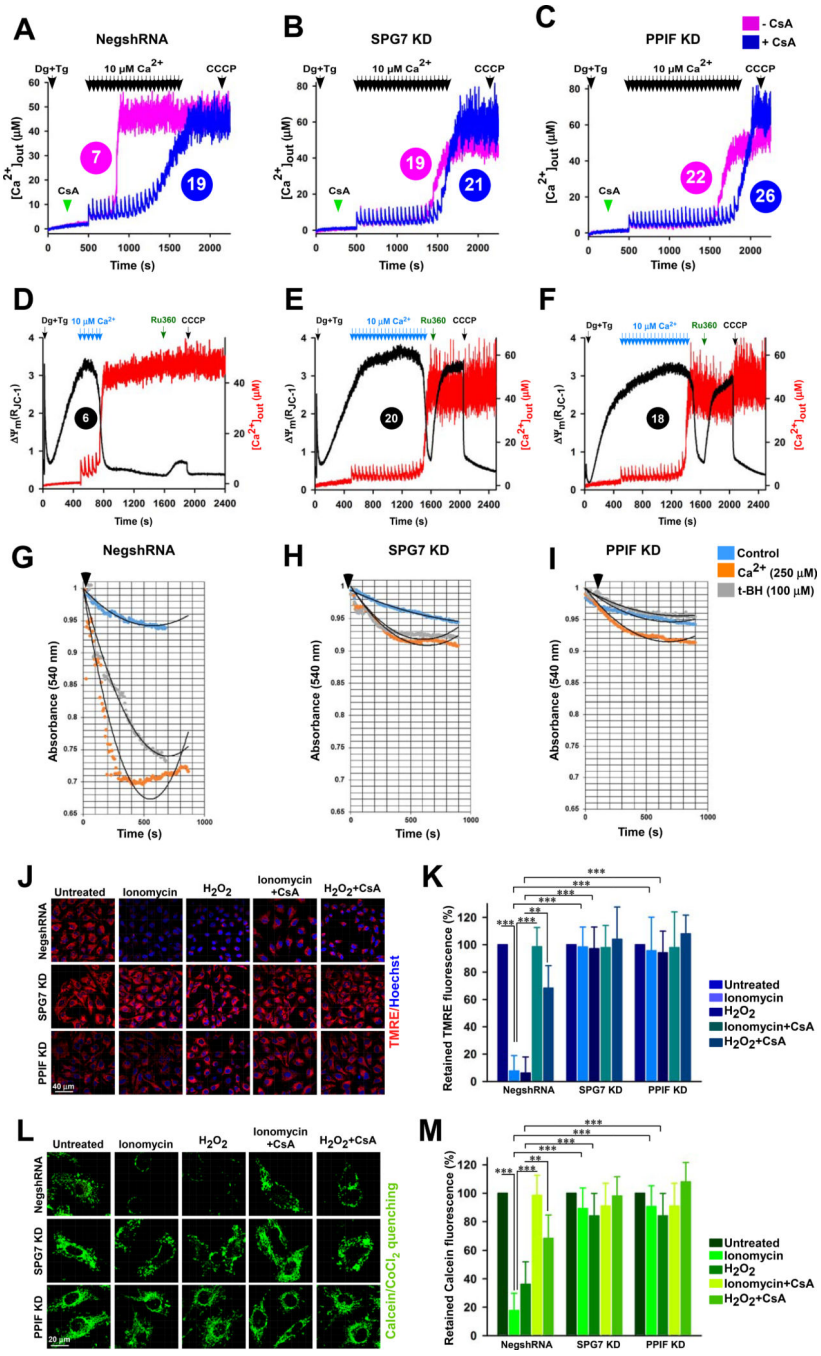

Figure 6. Ca^{2+} and Oxidant-Induced PTP Opening is a SPG7/PPIF-Dependent Process

(A–C) Representative traces of $[Ca^{2+}]_{out}$ clearance with (blue) or without CSA (pink) (5 μM) pretreatment at 250 seconds. $[Ca^{2+}]_{out}$ pulses and CCCP were delivered as indicated. n=3.

(D–F) Mitochondrial membrane integrity in Neg shRNA, SPG7 KD and PPIF KD cells. Permeabilized cells were then challenged with 10 μM Ca^{2+} bolus pulses after 500 s. Then, MCU blocker Ru360 (1 μM) and CCCP (3 μM) were added as indicated. n=3.

(G–I) Isolated mitochondria from Neg shRNA, SPG7 KD and PPIF KD cells were incubated with Ca^{2+} (250 μM) or t-butyl hydroperoxide (100 μM), and mitochondrial swelling was measured at 540 nm. The mean value traces were plotted with a polynomial fit. n=3–6.

(J) Neg shRNA, SPG7 KD and PPIF KD cells were pretreated with DMSO or CsA (5 μM) for 30 min prior to ionomycin (25 μM; 6 hrs) and H_2O_2 (0.8 mM; 6 hrs) treatment. $\Delta\Psi_m$ was measured using TMRE as an indicator.

(K) Quantification of mitochondrial TMRE fluorescence. Mean ± SEM; **p<0.01, ***p<0.001, n=3–4.

(L) Calcein quenching assay was performed to assess the PTP opening following Ca^{2+} overload and oxidative stress. Neg shRNA, SPG7 KD and PPIF KD cells were treated as in J. Calcein fluorescence was measured by confocal microscopy.

(M) Quantification of mitochondrial calcein fluorescence. Mean ± SEM; **p<0.01, ***p<0.001, n=3–4. See also Figures S6 and S7.

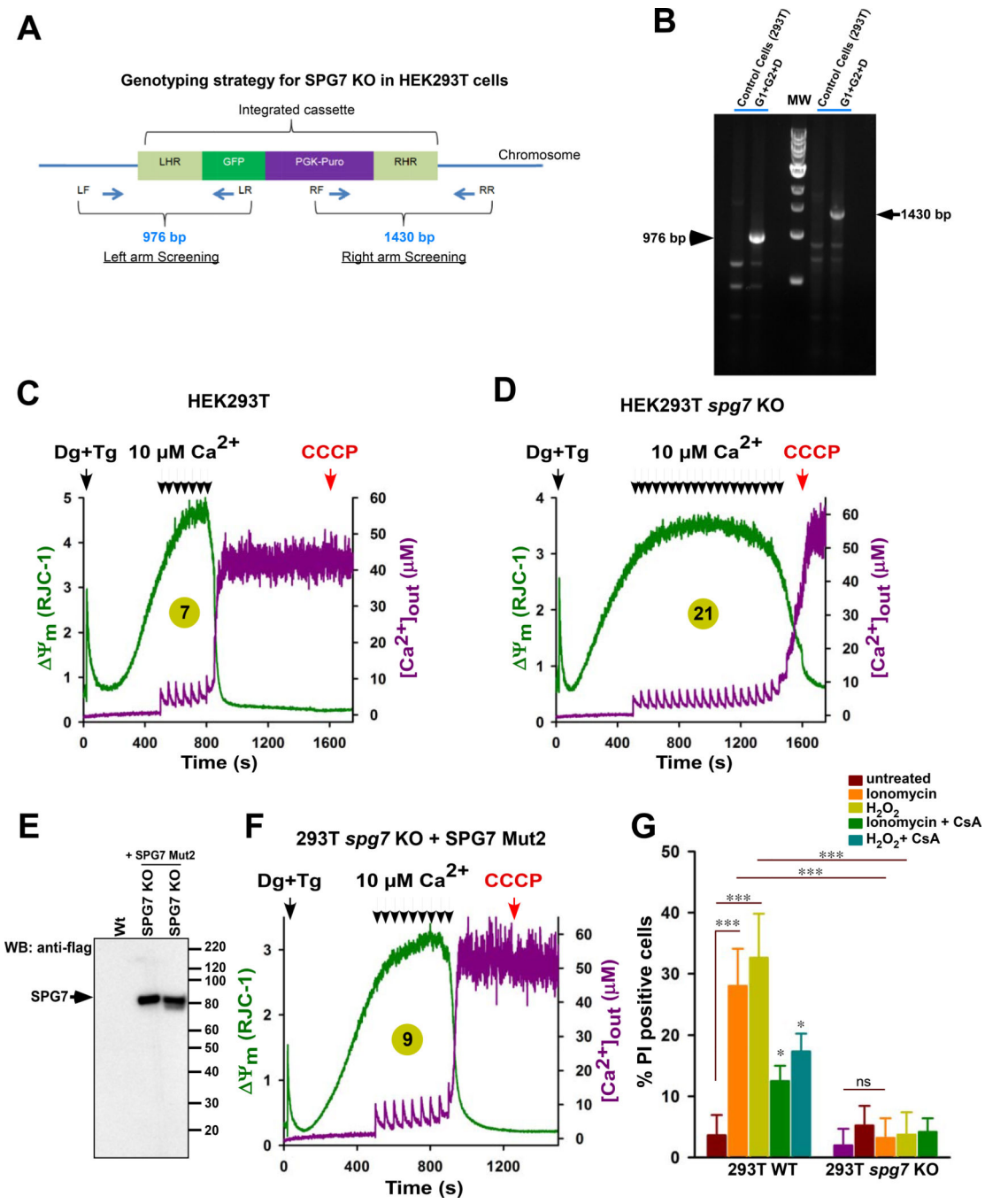

Figure 7. CRISPR/Cas9-Mediated *spg7* Knockout Mitochondria Retained High $[Ca^{2+}]_m$ and are Resistant to Cell Death

(A) Genotyping strategy for CRISPR/Cas9-Mediated *spg7* KO in HEK293T cells.

(B) Representative agarose gel image depicts the predicted targeting PCR products.

(C and D) Representative traces of $[Ca^{2+}]_{out}$ clearance (magenta) and $\Delta\Psi_m$ (green) of wild-type (left) and spg7 knockout 293T cells (right).

(E) Western blot depicts the reconstitution of SPG7 Mut2 in spg7 knockout 293T cells.

(F) Representative trace of spg7 knockout 293T cells expressing SPG7 proteolytic domain mutant2 (SPG7 Mut2). n=3.

(G) Quantification of cell death as PI positive cells. Mean ± SEM; *p<0.05, ***p<0.001, ns, not significant. n=3–4. See also Figures S7.